LIFTING SURFACE THEORY FOR A HELICOPTER ROTOR IN
FORWARD FLIGHT

H. Tai
NASA Langley Research Center
Hampton, Virginia 23665

Harry L. Runyan
College of William and Mary
NASA Langley Research Center
Hampton, Virginia 23665

ABSTRACT

A lifting surface theory has been developed for a helicopter rotor in forward flight for compressible and incompressible flow. The method utilizes the concept of the linearized acceleration potential and makes use of the vortex lattice procedure. Calculations demonstrating the application of the method are given in terms of the lift distribution on a single rotor, a two-bladed rotor, and a rotor with swept-forward and swept-back tips. In addition, the lift on a rotor which is vibrating in a pitching mode at 4/rev is given. Compressibility effects and interference effects for a two-bladed rotor are discussed.

INTRODUCTION

Rotating lifting surfaces are an integral part of the propulsive unit of every aeronautical and nautical vehicle, from the compressor and turbine blades of jet engines, the pumps for rocket engines, to propeller and helicopter rotors. The aerodynamics of these rotating elements has been under extensive study since the advent of the airplane and with a combination of experimental and analytical approaches, succcessful designs have been achieved. In many cases, two-dimensional theory has been used, usually modified by an assumed spanwise distribution, and inflow velocities. This paper presents a compressible, lifting surface method for a helicopter rotor in forward flight within the limits of linearized theory.

The method is based on the concept of the acceleration potential, originally introduced by Kussner (1941). The method was first applied to an oscillating wing in uniform translatory motion including effects of compressible flow by Runyan and Woolston (1957). The acceleration potential approach has now become standard for the determination of the unsteady aerodynamic forces for flutter studies of lifting surfaces in rectilinear motion.

The first use of the acceleration potential approach for a rotating system was made in a paper by Hanaoka (1962) for the loading on a marine propeller in incompressible flow. The acceleration potential has been used in the past in studying the propeller noise problem, but in all of these noise propagation cases the problem was specialized early in the analytical development to the so-called far-field case usually

with a stationary observer, whereas the lifting surface theory is essentially concerned with the details of the near-field case for a co-moving observer as well as the satisfaction of certain of certain boundary conditions. Runyan (1973) utilized the acceleration potential approach to obtain a solution to the oscillating propeller in compressible flow. Dat, (1973), has derived a general expression for an acceleration doublet for any motion. Pierce and Vaidyanathan (1983) have treated the helicopter rotor in forward flight using the method of matched asymptotic expansion for the incompressible case. The procedure developed here involves the precise numerical integration over the surface of the rotor in a time frame. The method sets forth a formulation of a fundamental three dimensional, compressible, unsteady aerodynamic theory for propellers and helicopter rotors.

The next section contains a brief derivation of the fundamental equations, including a discussion of some implications of the equations. The third section contains a description of the method of solution. Finally, the results of some calculations for the several specific examples are given.

SYMBOLS

A'	rotor blade area
A_{nm}	aerodynamic influence coefficients
A_n, B_n	Fourier coefficients
c	speed of sound
C	chord of rotor
C_T	thrust coefficient per blade (thrust/$\pi \rho \Omega^2 R_t^4$)
$\vec{D}$	vector distance from doublet to downwash point
D	absolute value of $\vec{D}$
$\hat{D} = \vec{D}/D$	unit vector of $\vec{D}$
I	value of singular integral
K	kernel function
$\vec{n}$	unit vector at downwash point, normal to velocity vector
$\vec{n}_0$	unit vector at doublet point, normal to velocity vector
ℓ, m, n	direction cosines of $\vec{n}$
ℓ_0, m_0, n_0	direction cosines of $\vec{n}_0$
p	pressure
$\vec{x}_0$	position vector of doublet from inertial frame origin
$\vec{x}$	position vector of downwash point from inertial frame origin

q	source or doublet strength
R_t	rotor tip radius
R_s	rotor root radius
r	distance of downwash point along the span
r_0	distance of doublet along the span
r_u	upper limit of spanwise panel
r_ℓ	lower limit of spanwise panel
$\hat{r}_0$	distance of doublet along span at singular point time
t	field time
U	velocity of rotor system, parallel to x-axis, positive in negative x-direction
$\vec{V}$	velocity at downwash points
V_n	velocity component of $\vec{V}$ at the downwash point normal to the rotor leading edge
$\vec{V}_0$	velocity of doublet
W	velocity of rotor system, parallel to z axis
w_n	downwash velocity
x_α	distance from pitch axis to downwash point
x,y,z	Cartesian coordinates of downwash point
x_0,y_0,z_0	Cartesian coordinates of doublet position
α	twist angle at downwash point
α_0	twist angle at doublet position
α_r	angle of axis of rotation relative to z-axis
$\vec{\beta}$	V_0/c
$\dot{\vec{\beta}}$	$\dot{\vec{V}}_0/c = \dfrac{1}{c}\dfrac{\partial \vec{V}_0}{\partial \tau}$
θ	angular position of blade at time t
θ_0	angular position of blade at time τ
θ_w	blade angle of attack
θ_R	blade angle relative to plane of rotation
μ	advance ratio
ρ	air density
τ,τ_0	time
$\hat{\tau}$	time at which integrand in Eq. (24) becomes singular
ϕ	velocity potential
Ψ_s	source acceleration potential
Ψ_D	doublet acceleration potential
ψ	azimuth angle
Ω	rotation speed of rotor
ω	vibration frequency of rotor

BASIC FORMULATION

The formulation of the aerodynamic equations is based on the linearized acceleration potential approach. The fluid is considered perfect, with no separation and the formulation is based upon the assumption of small perturbations. The wake created by the lifting rotor is assumed to lie in the skewed helical path taken by the rotor blade. One reason for adopting the acceleration potential approach is that the pressure discontinuity occurs only on the surface of the blade and thus the boundary conditions need only be applied on the blade surface and not throughout the wake. The blade is treated as a very thin surface of discontinuity across which a pressure jump occurs. Th effect of compressibiity is taken into account by utilizing the complete linearized potential for a lifting doublet, along with the effects of retarded time.

As shown in Fig. 1, an inertial coordinate system has been used in which the origin of coordinates is fixed to a point on the ground. The helicopter rotor is moving in the negative x-direction with velocity U, in the positive z-direction with velocity W and is rotating counter clockwise with a constant angular velocity Ω. A point of interest on the rotor blade is designated by the radius vector $\vec{X}_0(\tau)$ from the origin of the ground based coordinate system.

Let Ψ be the acceleration potential of a source (or doublet), the perturbation pressure is then given by

$$p = -\rho\Psi \qquad (1)$$

This expression represents the pressure p at point $\vec{X}$ due to a single source (or doublet) located at $\vec{X}_0$. The potential Ψ contains a constant "q" which represents the strength of the source and thus the magnitude of the pressure. In this form, there is no boundary condition available to determine the value of "q" and the resulting pressure. Recourse can be made to the velocity potential, since the spatial derivative of a velocity potential represents a velocity. The relationship between the pressure and velocity potential for an inertial coordinate system is

$$p = -\rho\frac{d\phi}{dt} \qquad (2)$$

where $\dfrac{d\phi}{dt}$ is the substantial derivative. Dropping out the second order terms and integrating with respect to field time results in

$$\phi(t) = \int_{-\infty}^{t} \Psi(t')\,dt' \qquad (3)$$

The acceleration potential Ψ_s satisfies the wave equation

$$\nabla^2\Psi_s - \frac{1}{c^2}\frac{\partial^2\Psi_s}{\partial t^2} = -4\pi\,f(\vec{X},t) \qquad (4)$$

where $f(\vec{X},t)$ is a source distribution. Furthermore, if the path of an isolated source is a function of time variable, $\vec{X}_0(t)$, then $f(\vec{X},t) = \delta(\vec{X} - \vec{X}_0)$ where δ is the delta function.

Using the Green's function formulation the acceleration potential expression for a moving source, Ψ_s can be written as (Morse and Feshbach, 1978, p. 841)

$$\Psi_s(\vec{X},t) = \frac{q(\vec{X}_0,\tau)}{4\pi|\vec{X}_0 - \vec{X}(\tau)|\left|1 - \dfrac{\vec{V}_0(\tau)\cdot[\vec{X} - \vec{X}_0(\tau)]}{c|\vec{X} - \vec{X}_0(\tau)|}\right|} \quad (5)$$

where $\vec{X}_0(\tau)$ designates the position of the source at time τ, $\vec{X}$ is the position of the field point at the time t, $\vec{V}_0(\tau)$ is the velocity of the source point at time τ, c is the speed of sound and q is the strength of the source. An auxiliary equation which relates the time interval $(t - \tau)$ to the distance between the two points is

$$t - \tau = \frac{|\vec{X} - \vec{X}_0(\tau)|}{c} \quad (6)$$

which is usually referred to as the causality condition. Eq. (5) expresses the potential as an explicit function of τ, and only through Eq. (6) as an implicit function of t ans $\vec{X}$. From Eq. (3), the velocity potential due to a moving source is

$$\phi_s(t) = \int_{-\infty}^{t} \Psi_s(t')\, dt' = \int_{-\infty}^{t} \frac{q(\tau')}{4\pi[D - \vec{D}\cdot\vec{\beta}]_{t'}}\, dt' \quad (7)$$

$$= \int_{-\infty}^{\tau} \frac{q(\tau')}{D(\tau')}\, d\tau',$$

where $\vec{D} = \vec{X} - \vec{X}_0$, $D = |\vec{D}|$

and $dt' = [1 - \dfrac{\vec{D}\cdot\vec{\beta}}{D}]\, d\tau'$

The quantities τ', t' and t, τ satisfy Eq. (6).

By definition, the doublet velocity potential ϕ_D of a doublet aligned along $\vec{n}_0$ can be written as

$$\phi_D(t) = \frac{\partial}{\partial n_0} \phi_s(t) = \vec{n}_0 \cdot \nabla_{\vec{X}_0} \phi_s = -\vec{n}_0 \cdot \nabla_{\vec{X}} \phi_s \quad (8)$$

$$= \lfloor \frac{\vec{n}_0 \cdot \vec{D}}{4\pi c(D-\vec{\beta}\cdot\vec{D})}\, \frac{q}{D} \rfloor_\tau + \int_{-\infty}^{\tau} q \frac{\vec{n}_0 \cdot \vec{D}}{4\pi D^3}\, d\tau'$$

Note that for incompressible flow, $c \to \infty$, the first term $\to 0$ and the integral remains unchanged except for the upper limit where $\tau = t$.

To obtain the final equation for downwash Δw_n, a second directional derivative is required. This derivative is taken normal to the flight path at the location of the downwash point, as follows

$$\Delta w_n = \frac{\partial \phi_D}{\partial n} = \vec{n} \cdot \nabla_{\vec{X}} \phi_D$$

to obtain

$$\Delta w_n = \frac{q}{4\pi c D^2[1-\hat{D}\cdot\vec{\beta}]} \{\vec{n}\cdot\vec{n}_0 + \vec{n}_0\cdot\dot{\vec{\upsilon}}\,\vec{n}\cdot\hat{n}$$

$$+(\vec{n}_0\cdot\vec{\beta}\,\vec{n}\cdot\hat{D} - \frac{\vec{D}}{c}\cdot\vec{n}_0\,\vec{n}\cdot\hat{D}$$

$$- \vec{n}_0\,\hat{D}\,\vec{n}\cdot\hat{D} + \vec{n}_0\cdot\hat{D}\,\vec{n}\cdot\vec{\beta})/(1 - \hat{D}\cdot\vec{\beta}) \quad (9)$$

$$-(\vec{n}_0\cdot\hat{D}\,\vec{n}\cdot\hat{D}[1-\beta^2+\frac{\vec{D}}{c}\cdot\vec{\beta}+\frac{\dot{q}}{qc^2 D}])/(1 - \hat{D}\cdot\vec{\beta})\}\tau_0$$

$$+ \frac{1}{4\pi} \int_{-\infty}^{\tau_0(r_0)} q\,[\frac{\vec{n}\cdot\vec{n}_0 - 3\vec{n}_0\cdot\hat{D}\vec{n}\cdot\hat{D}}{D^3}]\, d\tau$$

Eq. (9) gives the downwash at a field point (x, y, z, t) due to a doublet placed at a point (x_0,y_0,z_0,τ) having a strength q. In order to represent a lifting surface such as a rotor, it is necessary to distribute the doublets over the lifting surface and integrate over the surface to obtain the downwash at a field point. If the downwash is known, the quantity "q" can be determined. Letting K be the expression on the RHS of Eq. (9), the final equation is

$$w_n = \iint_{A'} K\, dA' \quad (10)$$

where A' is the area of the rotor surface. The LHS, w_n, represents the known boundary condition and is the velocity normal to the velocity vector at the downwash point. By using the no flow condition for the velocity perpendicular to the blade surface, the velocity component in the $\vec{n}$ direction is $V_n \tan\theta_w$ or

$$w_n(r,t) = V_n\tan\theta_w = \iint_{A'} K\, dA' \quad (11)$$

where V_n is the velocity component of V at the downwash point and is normal to the rotor leading edge and θ_w is the angle of attack. Thus the problem requires setting up a method of solution of Eq. (11) from which a value of q, the unknown doublet strength, can be determined which satisfy the known velocity boundary conditions w_n.

This represents a rather formidable computing task and the history of lifting surface theory even for non-rotating wings has centered on devising approximate methods to accomplish the integration in an economical manner. One method, termed the vortex lattice method, has been very successfully applied to aircraft wings, and is probably the more economical procedure of the many variants. This method was first demonstrated for the unsteady case by Runyan and Woolston (1957) and was later expanded by Albano and Rodden (1969). This is the method adopted in this paper and the application will be discussed later.

91

Specification of Coordinate System

The blade has the cord C and length $R_t - R_s$, R_s being distance to the the root of the blade, R_t is the distance to the tip of the blade. Let the blade momentarily coincide with the coordinate system along the positive x-axis at $t = 0$ and execute a counterclockwise rotation with angular velocity Ω while moving with velocity U along the negative x direction and velocity W along the positive z direction. Since the vortex lattice method has been adopted, the doublet point lies $C/4$ ahead and the downwash point lies $C/4$ aft of the section midchord. The position of the doublet point as well as the downwash point can be established as follows. The Cartesian components of the doublet position are

$$x_0 = -U\tau + r_0 \cos(\Omega\tau) - (C/4)\sin(\Omega\tau)\cos \alpha_0$$
$$y_0 = r_0 \sin(\Omega\tau) + (C/4) \cos(\Omega\tau)\cos \alpha_0$$
$$z_0 = W\tau + (C/4) \sin \alpha_0 \qquad (12)$$

where r_0 is the radial distance of the doublet along the span. With the substitution of $C \rightarrow -C$, $r_0 \rightarrow r$, $\tau \rightarrow t$ the position of the downwash point is given by

$$x = -Ut + r \cos(\Omega t) + (C/4) \sin(\Omega t)\cos \alpha$$
$$y = r \sin(\Omega t) - (C/4) \cos(\Omega t) \cos \alpha \qquad (13)$$
$$z = Wt - C/4 \sin \alpha$$

In Eqs. (12) and (13), the angles α, α_0 are the twist angles of the velocity vectors $\vec{V}$ and $\vec{V}_0$, respectively, defined by

$$\tan \alpha = \frac{W}{U \sin(\Omega t) + r\Omega}$$
$$\tan \alpha_0 = \frac{W}{U \sin(\Omega\tau) + r_0\Omega} \qquad (14)$$

The reference plane defined by the doublets and downwash points is a twisted surface. From Eq. (12) the doublet velocity can be computed, namely the time derivative of the position vectors.

$$\vec{V}_0 = \dot{x}_0 \vec{i} + \dot{y}_0 \vec{j} + \dot{z}_0 \vec{k}$$

The unit vector $\vec{n}_0$ is chosen to be perpendicular to the twisted surface created by the velocity vector $\vec{V}_0$ which is a function of r_0, through Eq. (14).

Express $\vec{n}_0$ as

$$\vec{n}_0 = \ell_0 \vec{i} + m_0 \vec{j} + n_0 \vec{k} \qquad (15)$$

where ℓ_0, m_0, n_0 are the directional cosines of the unit vector $\vec{n}_0$. It can be shown that

$$\ell_0 = \frac{W(U + r_0\Omega \sin(\Omega\tau) + (C/4)\Omega \cos(\Omega\tau)\cos \alpha_0)}{V_0' \sqrt{W^2 + V_0'^2}}$$

$$m_0 = - \frac{W(r_0\Omega \cos (\Omega\tau) - (C/4)\Omega \sin(\Omega\tau)\cos \alpha_0)}{V_0' \sqrt{W^2 + V_0'^2}} \qquad (16)$$

$$n_0 = \frac{V_0'}{\sqrt{W^2 + V_0'^2}}$$

where

$$V_0'^2 = (U + r_0\Omega \sin(\Omega\tau) + (C/4)\Omega \cos(\Omega\tau)\cos \alpha_0)^2$$
$$+ (r_0\Omega \cos(\Omega\tau) - (C/4)\Omega \sin(\Omega\tau)\cos \alpha_0)^2 \qquad (17)$$

By the same procedure, $\vec{n} = \ell\vec{i} + m\vec{j} + n\vec{k}$, where

$$\ell = \frac{W(U + r\Omega \sin(\Omega t) - (C/4)\Omega \cos(\Omega t)\cos \alpha)}{V' \sqrt{W^2 + V'^2}}$$

$$m = \frac{-W(r\Omega \cos(\Omega t) + (C/4)\Omega \sin(\Omega t)\cos \alpha)}{V' \sqrt{W^2 + V'^2}} \qquad (18)$$

$$n = \frac{V'}{\sqrt{W^2 + V'^2}}$$

and

$$V'^2 = (U + r\Omega \sin(\Omega t) - (C/4)\Omega \cos(\Omega t)\cos \alpha)^2$$
$$+ (r\Omega \cos(\Omega t) + (C/4)\Omega \sin(\Omega t)\cos \alpha)^2 \qquad (19)$$

the vector $\vec{D} = \vec{X} - \vec{X}_0$ defined in Eq. (7) can be expressed as

$$D = \{[U(t-\tau) + r \cos(\Omega t) - r_0 \cos(\Omega\tau)$$
$$+ (C/4)(\sin(\Omega t)\cos \alpha + \sin(\Omega\tau)\cos \alpha_0)]^2$$
$$+ [r \sin(\Omega t) - r_0 \sin(\Omega\tau) \qquad (20)$$
$$-(C/4)(\cos(\Omega t)\cos \alpha + \cos(\Omega\tau)\cos \alpha_0)]^2$$
$$+ [W(t-\tau) - (C/4)(\sin \alpha_0 + \sin \alpha)]^2\}^{1/2}$$

With the substitution of the quantities, the integral Eq. (11) was solved for the unknown $q(r_0,\tau)$ by using a collocation process based

on the vortex lattice assumption. The kernel is singular when $D = 0$, and this was handled by use of the finite part technique.

SOLUTION OF INTEGRAL EQUATION

In following the vortex lattice technique the rotor is divided into a number of predetermined panels, both spanwise and chordwise, In each chordwise panel, a line of doublets of unknown strength q_i is located at the 25% chordwise location of the particular panel, and the downwash is evaluated at the point located at 75% chordwise location of the panel. Therefore, a collocation procedure is used to obtain a set of equations in terms of the unknown loadings q_i. It is also assumed that the spanwise loading q_i is constant along each of the panels. A set of equations is thus obtained as shown below.

$$w_n = \sum_m A_{nm} q_m \qquad (21)$$

where $A_{nm} = \int_{r_\ell}^{r_u} K_{nm} \, dr_0$ and where n refers to

the downwash point and m refers to the vortex lattice. The kernel K is a complicated function which involves an integration over τ.

The term $q(r_0, \tau)$ represents the strength of the doublet located at r_0 and at time τ, and is proportional to the unknown loading. In order to account for unsteadiness, a solution was formulated to take into account the time variation of the strength of the wake. This was done by assuming a Fourier series of the form

$$q(r_0, \tau) = A_0 + \sum_1^m (A_n \cos(n\Omega\tau) + B_n \sin(n\Omega\tau)) \quad (22)$$

If $q(r_0, \tau)$ is assumed to be a function of r_0 alone, which means that the wake strength does not vary with time, the Fourier series reduces to $q(r_0) = A_0$. A solution obtained with this approximation is termed the quasi-steady solution.

This series was inserted in the basic equation and integrated with respect to τ. However, there were more unknowns than simultaneous equations to solve for the unknowns. The additional required equations were obtained by evaluating Eq. (11) at a number of azimuth locations. For instance if $m = 1$, then

$$q(r_0, \tau) = A_0 + A_1 \cos\Omega\tau + B_1 \sin\Omega\tau. \qquad (23)$$

The azimuth was divided into equal segments of $120°$ and the proper boundary conditions applied at $\psi = 0°$, $120°$, and $240°$ thus providing the necessary additional equations.

Numerical Integration of Kernel

The integration was performed by numerical integration, except for the area surrounding the

singularity. The integration domain was divided into areas as shown in Fig. 2. Areas 1-4 (hatched) were computed numerically using a two-dimensional Romberg integration (Davis and Rabinowitz, 1967) and the contribution of the singular region (unhatched) was obtained in closed form by consideration of the finite part as shown in the next section.

Treatment of Singular Term in Integral - The integral in the downwash equation, Eq. (11), is singular when $D \to 0$ and produces a complication which must be treated properly. It should be remembered that the integration path along "τ" is the path the doublet has taken in arriving at the final doublet point at $(c/4, r_0)$ measured in the local blade coordinates and can be considered as the wake. The integration takes place along the path from $-\infty$ to the final doublet position at τ_0. The distance D is the distance from the integration point at time τ to the downwash point at $\vec{x}$.

There is a particular set of values of r_0 and τ for which the denominator D approaches zero, thus resulting in an infinite integrand. The singular part of the Eq. (11) is

$$I = \int_{r_\ell}^{r_u} \int_{\tau_1}^{\tau_2} \frac{\vec{n} \cdot \vec{n}_0 - 3(\hat{D} \cdot \vec{n})(\hat{D} \cdot \vec{n}_0)}{D^3} \, d\tau \, dr_0 \quad (24)$$

As $\vec{D} \to 0$ at the downwash point, $\hat{D}$ becomes perpendicular to $\vec{n}$, therefore, at the singular point, the second term is zero and will be neglected in the treatment of the singularity. However, this second term is retained in all of the numerical integrations involving Areas 1-4 since it represents an important contribution particularly when the blade is passing over a trailing wake.
The time and distance at which the integral I becomes singular are designated by $\hat{\tau}$ and $\hat{r}_0$. The domain of the integration in Eq. (24) consists of a rectangle in which the duration $\tau_2 - \tau_1$ is kept extremely small. In other words, the integration is performed along a slit in r_0, over which the 2nd term in Eq. (24) is negligible. Therefore the integral I can be approximated by

$$I = \int_{r_\ell}^{r_u} \int_{\tau_1}^{\tau_2} \frac{\vec{n} \cdot \vec{n}_0}{D^3} \, d\tau \, dr_0 \qquad (25)$$

Furthermore, noticing that D^2 is quadratic in r_0, if α_0 is independent of r_0, then the integration on r_0 can be performed analytically. This can be achieved by recognizing that in the vortex lattice method, the rotor is divided into spanwise panels from r_ℓ to r_u. If these spanwise panels are small then the variation in α_0 is small.

$$\frac{d\alpha_0}{dr_0} = -\frac{W\Omega}{(U \sin\theta_0 + r_0\Omega)^2 + W^2} \qquad (26)$$

If the value of α_0 is approximated by its mid panel value, it is possible to integrate Eq. (24), in closed form in the r_0 direction. This is quite acceptable in the helicopter mode,

because $d\alpha_0/dr_0$ is in the order of magnitude 10^{-3} or smaller. The value $\hat{n}_0$ is also a function of r_0, but in the region of the singularity it has a very small variation and is evaluated at the singular position, $(\hat{\tau},\hat{r}_0)$. Performing the r_0 integration results in the form

$$I = \int_{\tau_1}^{\tau_2} \frac{g(\tau)}{f(\tau)} \, d\tau \qquad (27)$$

where $g(\tau)$ is a function containing all the non-singular part after performing the r_0 integration and $f(\tau) = 0$, at

$\tau=\hat{\tau}$ $(\tau_1 < \hat{\tau} < \tau_2)$. It can be argued physically that since the quantity $D(\tau,r_0; t,r)$ as well as its modified form $f(\tau)$ (after tegration over r_0) represents the distance between two points in space it must be positive and real for all its arguments, and never become negative. Denote the value of r_0 and τ at which D becomes zero as $\hat{r}_0$ and $\hat{\tau}_0$. Thus, in the neighborhood of $\hat{\tau}$ the function $f(\tau)$ behaves like a parabolic function and has a second order zero.

Expanding $f(\tau)$ in a Taylor series about the singular point $\hat{\tau}$ results in

$$f(\tau) = f(\hat{\tau}) + f'(\hat{\tau})(\tau-\hat{\tau}) + f'(\hat{\tau}) (\tau - \hat{\tau})^2/2 +\ldots \qquad (28)$$

Since $\hat{\tau}$ is a second order zero

$$\text{and} \qquad f(\hat{\tau}) = f'(\hat{\tau}) = 0 \qquad (29)$$

Eq. (29) has been verified numerically. If only the square term is kept in Eq. (28), Eq. (27) can be written as

$$I = \int_{\tau_1}^{\tau_2} \frac{2}{f''(\hat{\tau})} \left[\frac{g(\hat{\tau})}{(\tau-\hat{\tau})^2} + \frac{g'(\hat{\tau})}{(\tau-\hat{\tau})} + \frac{g''(\hat{\tau})}{2} \right] d\tau \qquad (30)$$

In Eq. (30), if τ_2 and τ_1 are chosen symmetrically about $\hat{\tau}$, then the odd derivative terms integrate to zero. Futhermore, the third term can be neglected since $g''(\hat{\tau})$ is small. The major contribution comes from the first term. Then using the standard integration technique (Mangler, 1952) the final result for the integral is

$$I = - \frac{g(\hat{\tau})}{f''(\hat{\tau})} \frac{4}{\Delta\tau} \qquad (31)$$

where $2\Delta\tau = \tau_2 - \tau_1$ and $\tau_1 < \hat{\tau} < \tau_2$.

A numerical problem arises because the finite part integration results in a negative number which is close to the total of the surrounding numerical integration areas which are positive. Thus, it is necessary to take the difference between large numbers, and the final integration accuracy is dependent on the accuracy of the two integrations. On the one hand, the numerical integration is more accurate

as $\Delta\tau$ is kept large because the very large values of the integrand near the singularity are avoided. On the other hand, regarding the finite part integration, the denominator was expanded in a Taylor series about the singular point, $\hat{\tau}$. Therefore, it is desirable to maintain $\Delta\tau$ as small as possible to keep within the limits of the applicability of the series expansion. Numerous calculations were made, varying $\Delta\tau$ until a reasonable convergence was found. This value was found to be $.01(t-\hat{\tau})$, i.e. 1% of the time difference. Actually, there is very little difference between 1% or 10% of the time difference and the computing time and cost is considerably reduced by using 10%. For trend studies 10% is recommended principally to reduce computer costs. Howcver, for final design type analysis, a smaller value of time difference $\Delta\tau$ is more appropriate.

For the spanwise direction, Δr_0 is also an integration limit variable. The finite part integral was obtained by approximating the angle of twist of the velocity vector across a segment by assuming it constant across the segment, having a value as determined at the center of segment. Numerical experimentation indicates that for a helicopter, $\Delta r_0 = 0$ is satisfactory.

APPLICATION TO SPECIFIC EXAMPLES

The foregoing analysis has been applied to several specific examples which are given in Figs. (3) and (4). The following section presents results for several paneling configurations; e.g. 5 spanwise and 1 chordwise panels (designated (5-1)) and 7 spanwise and 3 chordwise (designated (7-3)). The rotor blade was maintained at a constant pitch setting of $\theta_R = .1$ radians for all the calculations.

Single Blade

In order to investigate the convergence of the method when using the vortex lattice procedure, the program was run for several chordwise and spanwise elements for the incompressible case. The thrust coefficient C_T vs. the azimuth angle is shown in fig. (5). (In all of the following plots for thrust coefficient vs. azimuth angle, the thrust was calculated for 16 uniformly spaced azimuth angles and each curve was faired using a cubic spline). The rotor was first divided into 5 spanwise and one chordwise (5-1) panel and the results are shown by the solid line. The chordwise division was increased to (5-2) and the results are shown by the long dashed line. It can be seen that very little change has taken place. The spanwise divisions were increased to (7-1) and the largest change occurred at $\psi = 0°$ where the difference in C_T is about 11%. Increasing the chordwise divisions to 3 (7-3) shows convergence of the (7-1) case to be very good.

An interesting phenomena occurs in the region of small azimuth angles. For $\psi=0$ to

$37°$, the lift increases to a local maximum at $\psi=37°$ then the lift abruptly falls to a local minimum for $\psi=60°$ and then rapidly increased to a maximum at $\psi=100°$.' A similar phenomenon is shown analytically by Eglof and Landgrebe (1983) in Fig. 60 of that report where a local minimum and a local maximum occur in the same range of azimuth angles, even though the geometry of the two blades and the flight conditions are different. Also, in Fig. 93 of the same report some test data shows a similar variation of loading in the same azimuth range.

The chordwise pressure distributions for the (7-3) case are presented in figure 6. It should be remembered that in using the vortex lattice method, the loading is concentrated at the location of the vortex which for the (7-3) case is located at .0833C, .416C, and .75C. The pressure was faired using a cubic spline through the three vortex locations and the known value of zero at the trailing edge. The distributions are given for 7 spanwise positions. In general, the curves exhibit the expected shape, having the largest values as the leading edge is approached. For the span distribution the values at $r/R_T = .85$ are slightly larger than the values at $r/RT = .95$,, indicating a falling off in the tip region.

From these concentrated forces, the section pitching moment can be calculated. Figure 7 presents these results for $\psi = 90$ degrees. The section moment was taken about the 1/4 C and a nose down moment is taken as positive. The pitching moment shows some rather dramatic changes along the span. The moment is nose up near the tip ($r/R_T = .95$), changes to a small nose down value, then becomes nose up for most of the inboard region. Integration of the moment would result in a total pitch moment up at $\psi = 90°$.

Swept Tip

The segments used for the vortex lattice for the swept tip studies were(5-1), where two equal segments were used in the tip region and three equal segments were used in the unswept inboard section. In Fig. 8 the lift is shown plotted against azimuth for the two sweep conditions and for zero sweep. In general, the three results show little difference. The sweptback configuration has a larger lift from $\psi = 300°$ to $40°$. For $\psi = 100°$ to $240°$, the swept forward configuration has a slightly larger lift. It appears that the total lift for one rotation for the swept-back case and the sweptforward case would give about the same lift as produced by the unswept rotor. In Fig. 9 the lift distribution along the rotor span is given for $\psi = 0°$. The major effect of sweep is concentrated at the tip, where the swept-back tip load is greater than both the unswept and sweptback cases . In fig. 10, $\psi = 180°$. Comparing to fig. 9, the swept-back tip load is larger than both the unswept and the swept-forward tips.

Blade Oscillating in Pitch

An example of unsteady loads on a rotor blade with (5-1) paneling which is oscillating in a pitching mode about the mid-chord at a frequency of 4 per revolution (120 cycles/sec) is given on fig. 11. For this case a 17 term Fourier series (m=8) was used to simulate the oscillating load, which was comprised of one constant term, 8 cosine terms, and 8 sine terms. The steady and unsteady rotor blade loading is given for one revolution. The blade was oscillated through an angle of .1 rad. about a mean angle of .1 rad. The effect of the oscillation is readily apparent as compared to the steady case. With the harmonic representation of the loading, the magnitude and phase of the several harmonic loads are easily determined. The magnitudes are plotted in Fig. 12. The only harmonic loads that were significantly changed from the steady case were the 3rd, 4th and 5th. Both the 3rd and 5th harmonics were increased and the 4th harmonic was dramatically increased. Another calculation was made for the non-oscillatory unsteady case and compared to the quasi-steady case. Virtually no difference was observed, indicating that, at least for this case, the rate of change of loading in a revolution of the blade is small enough so that the effect of a variable wake is negligible.

Compressible Effects (5-1)

For a one-bladed rotor, the effect of compressibility is illustrated in Fig. 13, in which the C_T is plotted against azimuth angle. The incompressible result is included for comparison. As expected, the compressible load is larger than the incompressible throughout one revolution. The effect is greatest in the region of the advancing blade and smallest in the retreating region as would be expected.

Two-Bladed Rotor in Compressible Flow (5-1 per blade)

The method has been extended to the two-bladed rotor for the compressible case and the results are shown in Fig. 14. The thrust coefficient C_T per blade is given vs. azimuth angle for a single bladed rotor and for a two-bladed rotor. For azimuth angles from $\psi = 20°$ to $120°$ the single blade rotor has a larger C_T. For $\psi = 120°$ to $260°$, the C_T on the one and two-bladed rotors are approximately the same. However, for $\psi = 260°$ to $340°$ a dramatic reduction in lift occurs for the two-bladed rotor as compared to the one bladed results. The lowest lift occurs at $\psi = 292°$ which places the other blade of the two-bladed rotor at $\psi = 112°$, the point of maximum lift on the other blade. Apparently the high lift on the blade at $\psi = 112°$ creates a very unfavorable induced velocity on the second blade at $\psi = 292°$ which requires the loading to go to zero in order to satisfy the boundary conditions at $\psi = 292°$.

CONCLUDING REMARKS

A linearized lifting surface theory including the effects of compressibility has been developed for a helicopter rotor in forward flight. The method utilizes the concept of the acceleration potential, and makes use of the vortex-lattice procedure for performing the required integrations. In addition, the method has been extended to include the effects of unsteady flow.

Sample calculations have been done for several cases. These include the effect of swept-back and swept-forward tip. The effect of these two tip configurations was minimal on the total loading for one revolution. However, the loading distribution changed considerably for several azimuth positions. A comparison of the thrust coefficient, C_T, of a one bladed rotor and a two bladed rotor was made. In the azimuthal range between 20° and 120°, the one bladed rotor showed higher lift. However between $\psi = 260^\circ$ to 340° the two bladed rotor indicated a lower C_T. Compressibility was investigated for one configuration. As expected, the effect was greatest in the advancing blade region ($\psi = 90^\circ$) and was minimal in the retreating blade region. The effect on C_T of a blade oscillating in pitch at 4/rev is given. The effect on the total blade lift is shown and the effect of the oscillation is readily apparent. The harmonic content was calculated and the greatest difference between the oscillatory and non-oscillatory cases was found in the 4th harmonic.

REFERENCES

Albano, E.; Rodden, W. P. 1969: A Doublet Lattice Method for Calculating Lift Distribution on Oscillating Surfaces in Subsonic Flows. AIAA Journal, Vol. 7, No. 2, pp. 279-285.

Dat, Roland 1973: The Lifting Surface Theory Applied to Fixed Wings and Propellers ONRA TP No. 1298.

Davis, P. J. and Rabinowitiz, P., 1967: Numerical Integration, Blaisdell Publishing Company.

Eyolf, T. A. and Landgrebe, A. J. 1983: Helicopter Rotor Wake Geometry and its Influence in Forward Flight, Vol. 1, NASA CR 3726.

Hanaoka, T. 1962: Hydrodynamics of an Oscillating Screw Propeller. ONR, ACR (92) (1962).

Kussner, Hans G. 1941: General Airfoil Theory. NACA TM 979.

Morse, P. M. and Feshback, H. 1978: Methods of Theoretical Physics, McGraw-Hill, Inc.

Mangler, K. W. 1952: Improper Integrals in Theoretical Aerodynamics.

Pierce, G. A.; and Vaidyanathan, A. R. 1983: Helicopter Rotor Loads Using Discretized Matched Asymptotic Expansions, NASA CR 166092.

Runyan, H. L., and Woolston, D. S. 1957: Method for Calculating the Aerodynamic Loading on an Oscillating Finite Wing in Subsonic and Sonic Flow. NACA TR 1322.

Runyan, H. L. 1973: Unsteady Lifting Surface Theory Applied to a Propeller and Helicopter Rotor, Ph.D. Thesis, Loughborough, University of Technology.
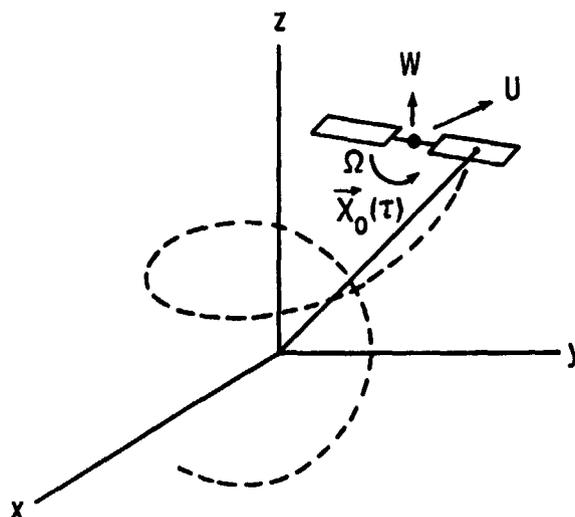
Fig. 1 Inertial Coordinate System

Fig. 2 Integration Areas

$U = 100$ ft/sec $\alpha_r = 0.05$ rad
$W = 5$ ft/sec
$\Omega = 30$ rad/sec $\mu = 0.17$
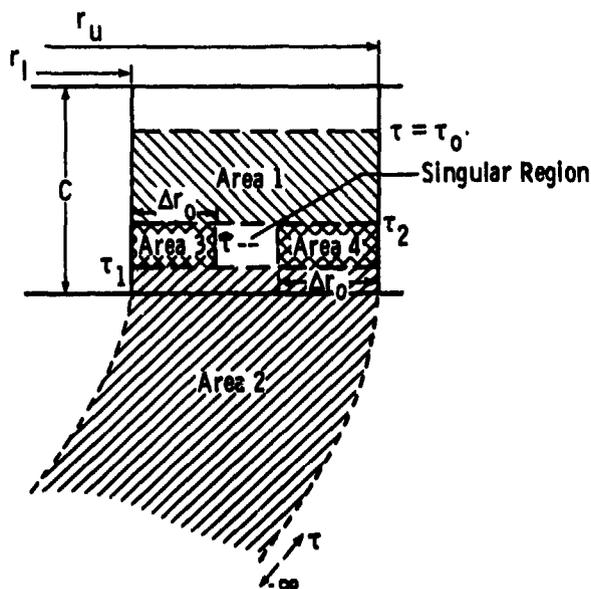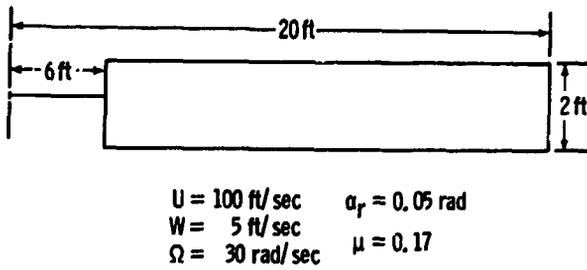
Fig. 3   Unswept Configuration and Input Parameters
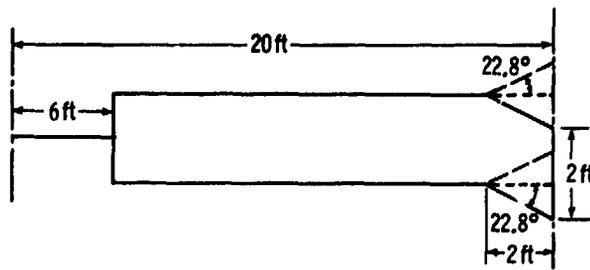
Fig. 4   Swept Tip Configurations
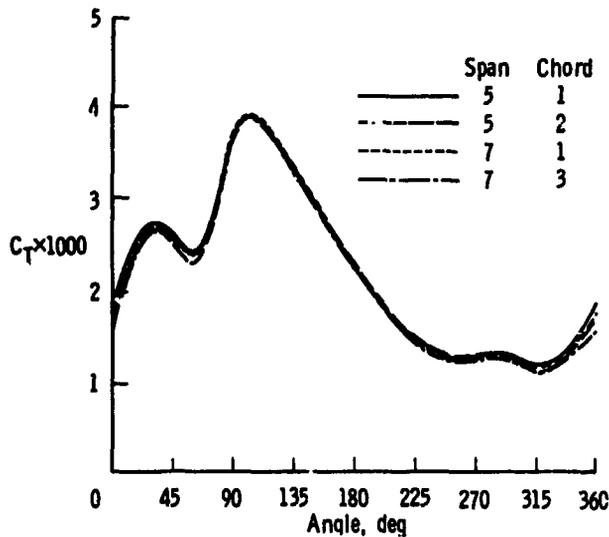
Fig. 5   Thrust Coefficient vs. Azimuth Angle for Four Panel Configurations for a Single Rotor Blade, incompressible, ($\mu = 0.17$, $\theta_\beta = 0.1$ rad, $\alpha_r = .05$ rad, $\Omega = 30$ rad/sec)
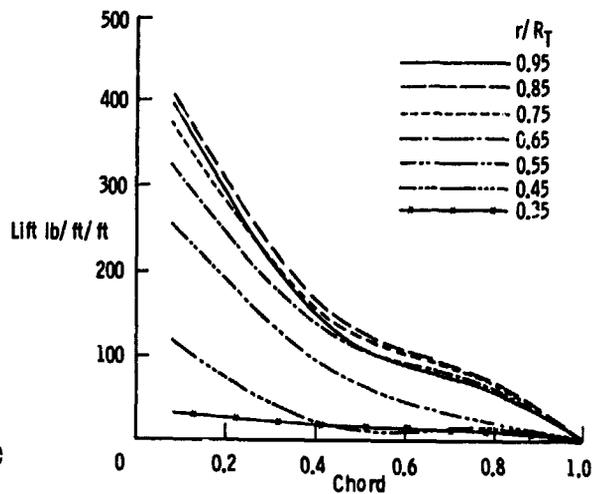
Fig. 6   Chordwise Pressure Distribution for Several Spanwise Locations, $\psi = 90°$, incompressible, ($\mu = .17$, $\theta_\beta = 0.1$ rad, $\alpha_r = .05$ rad, $\Omega = 30$ rad/sec)
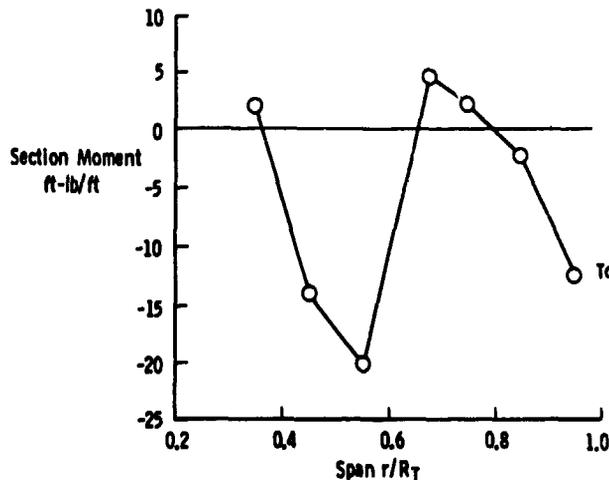
Fig. 7   Spanwise Section Moment Distribution about 1/4C - Positive Nose Down, $\psi = 90°$, incompressible, ($\mu = 0.17$, $\theta_\beta = 0.1$ rad, $\alpha_r = .05$ rad, $\Omega = 30$ rad/sec)
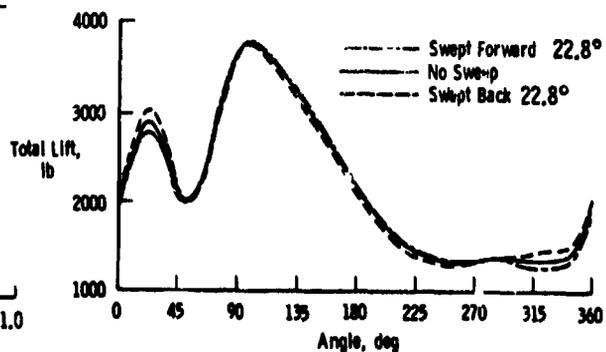
Fig. 8   Comparison of Lift on a Swept-Back Zero Sweep and Swept-Forward Blade, incompressible, ($\mu = 0.17$, $\theta_\beta = 0.1$ rad, $\alpha_r = .05$ rad, $\Omega = 30$ rad/sec)
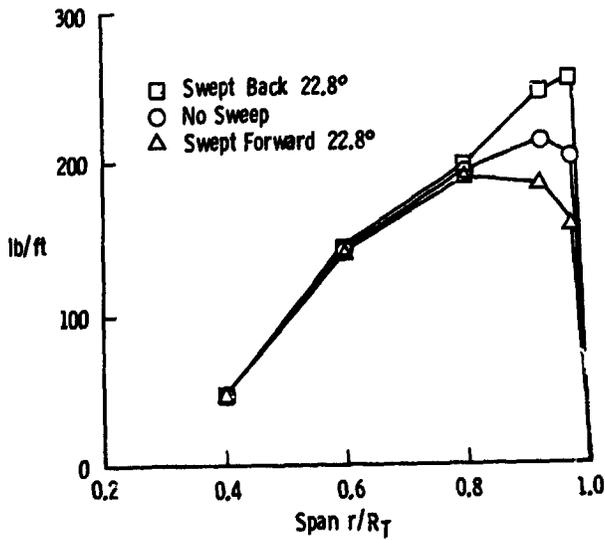
Fig. 9 Spanwise Section Lift Distribution for Swept-Tip Configurations, $\psi = 0°$, incompressible, ($\mu = 0.17$, $\theta_\beta = 0.1$ rad, $\alpha_r = .05$ rad, $\Omega = 30$ rad/sec)
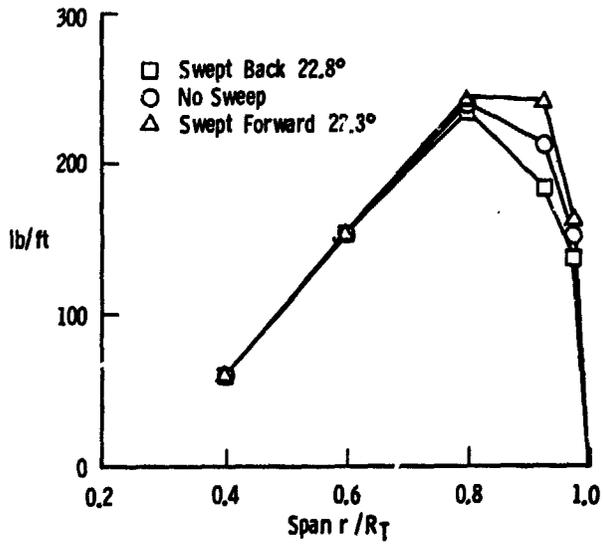
Fig. 10 Spanwise Section Lift Distribution for Swept-Tip Configurations, $\psi = 180°$, incompressible, ($\mu = 0.17$, $\theta_\beta = 0.1$ rad, $\alpha_r = .05$ rad, $\Omega = 30$ rad/sec)
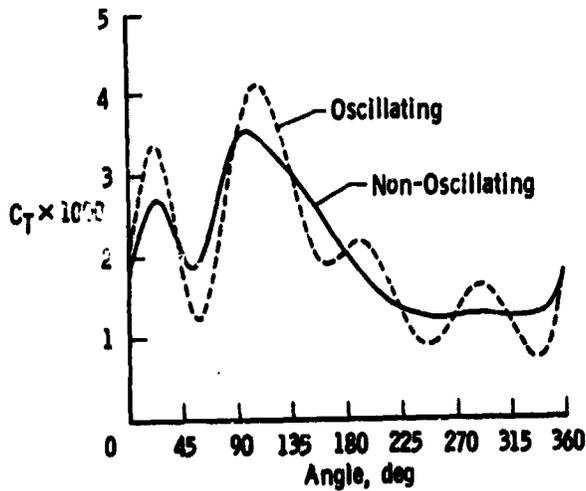
Fig. 11 Comparison of Lift on a Rotor Blade Oscillating in Pitch at 4/Rev. to the Lift on a Non-Oscillatory Blade, incompressible ($\mu = 0.17$, $\theta_\beta = 0.1$ rad, $\alpha_r = .05$ rad, $\Omega = 30$ rad/sec)
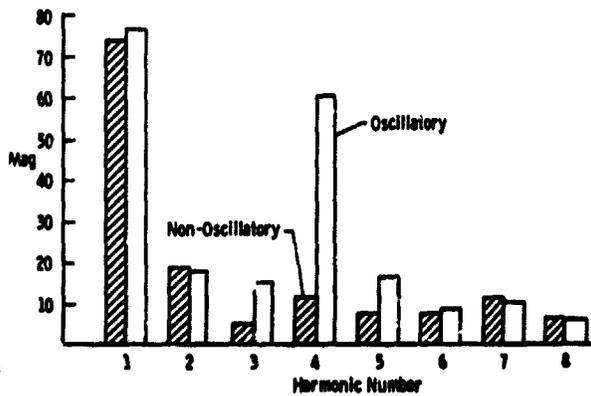
Fig. 12 Harmonic Content for Non-Oscillatory and Oscillatory Cases - $r/R_T = .95$, incompressible, ($\mu = 0.17$, $\theta_\beta = 0.1$ rad, $\alpha_r = .05$ rad, $\Omega = 30$ rad, sec)
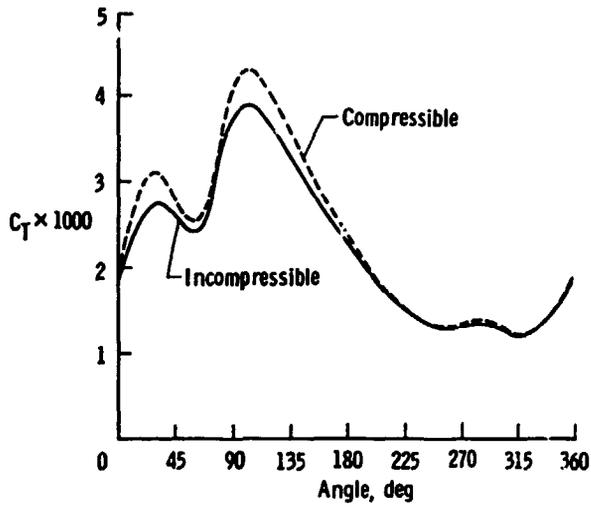
Fig. 13 Incompressible and Compressible Lift for One-Bladed Rotor, ($\mu = 0.17$, $\theta_\beta = 0.1$ rad, $\alpha_r = .05$ rad, $M_{TIP} = 0.54$)
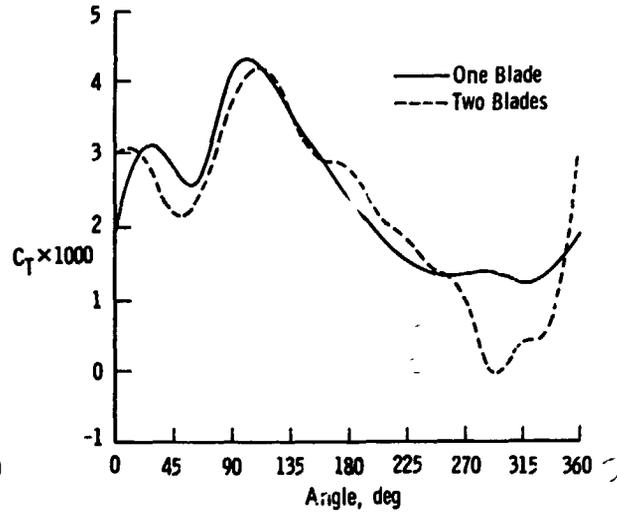
Fig. 14 Lift on Two-Bladed and One-Bladed Rotor vs. Azimuth Angle, compressible, ($\mu = 0.17$, $\theta_\beta = 0.1$ rad, $\alpha_r = .05$ rad, $M_{TIP} = 0.54$)

DISCUSSION
Paper No. 7

LIFTING SURFACE THEORY FOR A HELICOPTER ROTOR IN FORWARD FLIGHT
H. Tai
and
Harry L. Runyan

Bob Sopher, Sikorsky Aircraft: Just a couple of questions. One, you had a rigid rotor in this analysis?

Tai: Yes.

Sopher: There is no aeroelasticity and you went up to a μ of .17?

Tai: That's correct.

Sopher: First of all, I think that as soon as you put aeroelasticity in you are going to see different trends when you put sweep on in comparison without sweep.

Tai: Oh, sure.

Sopher: The second thing is at μ equal to .17 I think that the skewed helical wake will not be a very good approximation to the actual wake, which will be substantially distorted—more like a wake that you would get under hover conditions. So I question the utility of assuming a skewed helical wake.

Tai: As I pointed out this is a first cut. Of course later you can modify this by iteration processes. You can go back and calculate the wake and put it back again. Hopefully, that procedure would give you a better result.

Sopher: The third question is what advance ratios do you expect to apply the analysis up to?

Tai: The answer is I don't know. However, I would think that the higher forward speed would probably have a better answer. Because you don't depend on the wake that much.

Sopher: I question that because as you go up to higher speeds you are going to find that you run into situations where you get transonic flow on the advancing blade and I do not believe that the linear analysis will apply accurately under those conditions.

Tai: Perhaps you are right.

Sopher: As a matter of fact this research center has developed transonic flow analyses which apply to three dimensional lifting blades so I would say that the primary utility that I would see in this analysis is for hover applications where the linear analysis is valid, but you would have to use a distorted wake.

Tai: For hover cases you would really expect the wakes to stack up and then you end up with a very difficult mathematical problem. However, I guess from my past experience you probably can get the loading by some numerical procedure. For example, you can do extrapolation. Assuming a certain W and then you extrapolate for W = 0. I don't know. We don't have a clear understanding. I admit that.

Jim McCroskey, U.S. Army Aeromechanics Laboratory: You have made some nice progress on this approach since you talked with us a year or so ago. It's interesting; it's nice to see some results being generated for some realistic cases. I wanted to ask a couple of minor questions. I presume this blade is untwisted, is that right?

Tai: Yes.

McCroskey: How did you treat the reverse flow region?

Tai: The twist can be added on very easily because [we only have to] add on the boundary condition. To avoid a reverse phenomenon we deliberately use very large cutoff. You can see [that it is] six feet. We try to avoid that region.

McCroskey: In fact the sketch in the book is a little misleading because the cutout is more like 30% instead of the 10 or 15% [that appears in the figure]. So you just avoided it by having a root cut out.

Tai: Yes.

McCroskey: The final thing is on the influence of compressibility. Do you have some idea of what you predict in Figure 13; is that a larger effect than you would predict if you just used some kind of Prandtl-Glauert scaling on the incompressible solution?

Tai: Well, I guess we should be blamed for not making the abstract very clear. We used a very, very honest way of doing that. We didn't use any approximation at all. In other words, as I pointed out, you find the τ as function of r_o. In other words, you give it the radius of the doublet [and] you go there and find the τ which serves as your upper limit—which is not a trivial matter. To answer your question we say that we use true, honest compressibility effect.

McCroskey: But the question is how good would the Prandtl-Glauert type approximation be to what you actually calculated?

Tai: Well, to honestly answer that question—we don't know. We didn't check [it], but I think it is not very easy to check it out.

Bob Ormiston, U.S. Army Aeromechanics Laboratory: I want to commend your results. It looks like you have made some pretty good progress in the last year or so. The methods we are using now for routine rotor loads analysis are usually based on some fairly primitive assumptions like strip theory and 2-D airfoil coefficients and so forth and what we ultimately have to get to is very, very sophisticated, maybe, 3-D CFD kinds of analyses. It looks like what you've got is an intermediate type of analysis which may be very practical. My question is do you think there is a practical way to generalize the results you have gotten, say, to come up with generalized forcing functions for specific loading distributions, a family of loading distributions that you might be able to calculate and then not have to repeat the integration problem for each particular configuration that you are analyzing? Is there a practical way to do that?

Tai: Well to answer your question, the answer is yes. I did not mention that when we break the blade into different segments. Apparently the matrix is highly diagonal. In other words off diagonal matrix you can use less accurate methods to generate. Beyond that, to answer your question, I think in a practical sense we can generate those matrix elements and store them and only change the boundary conditions to do all the types of calculations. In other words, the answer is indeed it can be very practical.